Numerical Heat Transfer, Part B, 47: 257–275, 2005

ISSN: 1040-7790 print/1521-0626 online
DOI: 10.1080/10407790590901648

Taylor & Francis
Taylor & Francis Group

A MESHLESS METHOD BASED ON LEAST-SQUARES APPROACH FOR STEADY- AND UNSTEADY-STATE HEAT CONDUCTION PROBLEMS

Y. Liu, X. Zhang, and M.-W. Lu
Department of Engineering Mechanics, Tsinghua University, Beijing, People's Republic of China

The meshless method based on the least-squares approach, the meshless weighted least-squares (MWLS) method, is extended to solve conduction heat transfer problems. The MWLS formulation is first established for steady-state problems and then extended to unsteady-state problems with time-stepping schemes. Theoretical analysis and numerical examples indicate that larger time steps can be used in the present method than in meshless methods based on the Galerkin approach. Numerical studies show that the proposed method is a truly meshless method with good accuracy, high convergence rate, and high efficiency.

1. INTRODUCTION

In the recent decade, a new class of numerical methods, meshless methods (also called mesh-free methods), have been developing fast [1, 2]. Though most meshless methods originate from solid mechanics, they have been extended to solve problems of heat transfer and fluid flow, owing to their advantages over the traditional finite-element method (FEM), finite-volume method (FVM), and finite-difference method (FDM). Meshless methods rely only on a group of scatter points, which means not only that the burdensome work of mesh generation is avoided, but also more accurate description of irregular complex geometries can be achieved. Furthermore, the meshless approximation has higher smoothness, and no additional postprocessing is needed.

In the field of meshless methods for solving heat transfer problems, Cleary and Monaghan [3] employed smoothed particle hydrodynamics (SPH) with a Euler prediction-correction algorithm to analyze unsteady-state heat conduction problems in a finite slab; Chen et al. [4] solved unsteady-state heat conduction problems with a corrective SPH method; Onate et al. [5] developed a finite-point method (FPM) to solve convective transport problems; Chen [6] used a boundary particle method (BPM) with high-order fundamental and general solutions to analyze convection-diffusion problems with complex geometry; Liu and Yang [7] solved unsteady-state

Received 15 January 2004; accepted 16 July 2004.
The authors gratefully acknowledge the support of the National Natural Science Foundation of China with grant 10172052.
Address correspondence to Xiong Zhang, Department of Engineering Mechanics, Tsinghua University, Beijing 100084, People's Republic of China. E-mail: xzhang@tsinghua.edu.cn

NOMENCLATURE

$a_i(\mathbf{x})$, $\mathbf{a}(\mathbf{x})$	coefficient of basis function and its vector form	t_0	the origin of time
		u	temperature
c	specific heat	$\bar{u}$	specified temperature on the boundary
$d^{\max}$, $d_x^{\max}$, $d_y^{\max}$	size of the compact support		
$\mathbf{G}, \mathbf{K}$	system matrices of discretized equations	u_f	environmental temperature
		u_I, $\mathbf{U}$	nodal parameter and its vector form
h	convection heat transfer coefficient		
		u_0	initial temperature
k	thermal conductivity	$w_I(x)$	weight function
L	characteristic length	$\mathbf{x}$	vector of spacial coordinate
L_e	dimension of element (in finite-element method) or nodal distance (in meshless methods)	x, y	spacial coordinates
		α_1, α_2, α_3	penalty parameters
		Γ_1, Γ_2, Γ_3	boundaries
		Δt	size of time step
n	unit normal vector outward to the boundary	θ	parameter of time discretization scheme
$N_I(\mathbf{x})$	shape function	Π	functional to construct discretized equations
N_{node}	number of nodes		
$p_i(\mathbf{x})$, $\mathbf{p}(\mathbf{x})$	basis function and its vector form	ρ	density
		Ω	problem domain
$\mathbf{P}$	right-hand-side vector of the discretized equations	**Subscripts**	
$\bar{q}$	specified heat flux on the boundary	c	critical
		I, J	node indices
Q	heat source		
r	normalized radius	**Superscripts**	
R_0	residual of the governing equation	e	exact
		h	approximate
R_1, R_2, R_3	residuals of boundary conditions	n	time-step index
		num	numerical
t	time		

heat conduction problems with the element-free Galerkin method (EFGM) and the coupled EFGM-FEM in combination with a precise algorithm in the time domain; Singh et al. applied the EFGM in the heat transfer analysis of 2-D fins [8], 3-D steady-state [9], and transient [10] heat conduction problems, and composite heat transfer problems [11]. They studied the influences of different weight functions and different sizes of support domain in detail [11]. Sadat and his collaborators developed the diffuse approximation method (DAM) and utilized it to solve 2-D and 3-D laminar natural-convection problems [12, 13].

All the above meshless methods can be categorized into two groups according to their discretization scheme. The first group is Galerkin-based meshless methods (GBMMs), of which the EFGM proposed by Belytschko in 1994 [14] is a famous representative. In GBMMs, the highest order of derivatives is lowered by using a weak form of the original partial differential equations (PDEs). The accuracy of GBMMs is high, and good stability can always be obtained. The main shortcoming of GBMMs is that the integrals in the weak form must be evaluated properly. One way of evaluating integrals is to use a background mesh, which makes the method

not truly meshless; another is to use nodal integration [15], which results in significant errors because the divergence theorem used in the establishment of the weak form demands accurate integration [16]. In addition, because meshless shape functions are too complex to be expressed in closed form, a delicate background mesh and a large number of quadrature points are always employed, which decreases the efficiency seriously. As a consequence, GBMMs are much more computationally expensive than the FEM.

The other group of meshless methods is built on collocation schemes. The SPH, FPM, DAM, least-square collocation meshless method [17], and radial basis function (RBF) collocation methods [18–21] all belong to this group. These methods are very efficient and easy to program, but they usually suffer from poor stability, and the accuracy often goes down near the boundary.

The universal law of least squares can also be used for discretization. In fact, it has been introduced into the FEM successfully [22]. A new meshless method based on the least-squares approach, the meshless weighted least-squares (MWLS) method, was proposed to solve problems of elastostatics [23], wave propagation and large deformation [24]. The MWLS method is not bothered by instability as collocation-based meshless methods, and its accuracy and convergence rate are comparable to, or even better than, that of GBMMs [23]. At the same time, the MWLS method is an efficient algorithm, owing mainly to employing discrete functionals, which is feasible because integration is used only to average the residuals of the governing equations and boundary conditions in the least-sqaures approach, and the solution accuracy in the least-squares approach is less sensitive to the integration accuracy than in the Galerkin method [16].

In this article, the MWLS method is extended to solve problems of conduction heat transfer. The governing equation and boundary conditions are briefly investigated in Section 2; implementation of the MWLS method, including the meshless approximation scheme, the formulas for steady-state heat conduction equations and for unsteady-state heat conduction equations in combination with the time-stepping scheme, are derived in Section 3; numerical examples are demonstrated in Section 4; and some concluding remarks are presented in Section 5.

2. BASIC EQUATIONS OF HEAT CONDUCTION PROBLEMS

The distribution of temperature in the problem domain Ω is governed by the following equation:

$$\rho c \frac{\partial u}{\partial t} = k\nabla^2 u + \rho Q \qquad \text{in } \Omega \tag{1}$$

with boundary conditions

$$\begin{aligned} u &= \bar{u} && \text{on } \Gamma_1 \\ \mathbf{n} \cdot k\nabla u &= \bar{q} && \text{on } \Gamma_2 \\ \mathbf{n} \cdot k\nabla u &= h(u_f - u) && \text{on } \Gamma_3 \end{aligned} \tag{2}$$

where u represents the temperature; t stands for time; ρ and c are density and specific heat, respectively; k is the thermal conductivity; and Q is the heat source per unit

mass. Γ_1, Γ_2, and Γ_3 denote the first kind (specified temperature), the second kind (specified heat flux), and the third kind (convection heat transfer) of boundaries. $\bar{u}$ and $\bar{q}$ are the prescribed temperature and the prescribed heat flux on the corresponding boundaries, respectively. h is the convection heat transfer coefficient, and u_f is the environmental temperature. $\mathbf{n}$ is the unit normal vector outward to the boundary.

For the unsteady-state case, the following initial condition should also be specified:

$$u = u_0 \qquad \text{when } t = t_0 \tag{3}$$

For the steady-state case, the variable u is not a function of time t. Thus no initial condition is needed, and the governing equation is simplified as

$$k\nabla^2 u + \rho Q = 0 \tag{4}$$

3. IMPLEMENTATION OF MWLS METHOD

3.1. The Moving Least-Square (MLS) Approximation

In the MLS approximation, the function $u(\mathbf{x})$ is approximated by $u^h(\mathbf{x})$ as follows:

$$u(\mathbf{x}) \approx u^h(\mathbf{x}) = \sum_{i=1}^{m} p_i(\mathbf{x}) \cdot a_i(\mathbf{x}) = \mathbf{p}^{\mathrm{T}}(\mathbf{x}) \cdot \mathbf{a}(\mathbf{x}) \tag{5}$$

where m is the number of terms of the basis. $p_i(\mathbf{x})$ and $a_i(\mathbf{x})$ are the basis functions and the corresponding coefficient, respectively. The coefficient $a_i(\mathbf{x})$ is obtained by minimizing the difference between the local approximation and the function, which yields the quadratic form

$$J = \sum_{I=1}^{n} w_I(\mathbf{x}) \cdot \left[\mathbf{p}^{\mathrm{T}}(\mathbf{x}_I) \cdot \mathbf{a}(\mathbf{x}) - u_I\right]^2 \tag{6}$$

where $u_I = u(\mathbf{x}_I)$ is the nodal value of the function $u(\mathbf{x})$, and is also called nodal parameter since $u_I \neq u^h(\mathbf{x}_I)$ in MLS approximation. $w_I(\mathbf{x}) = w(\mathbf{x} - \mathbf{x}_I)$ is the weight function which is non-negative with a compact support associated with node $\mathbf{x}_I$ (a small neighborhood centered at the node $\mathbf{x}_I$) and maximum at node $\mathbf{x}_I$. n is the number of nodes whose weight functions are nonzero at the evaluation point $\mathbf{x}$. Minimizing functional J results in

$$\mathbf{A}(\mathbf{x}) \cdot \mathbf{a}(\mathbf{x}) = \mathbf{B}(\mathbf{x}) \cdot \mathbf{u} \tag{7}$$

where

$$\mathbf{A}(\mathbf{x}) = \sum_{I=1}^{n} w_I(\mathbf{x})\, \mathbf{p}(\mathbf{x}_I)\, \mathbf{p}^{\mathrm{T}}(\mathbf{x}_I) \tag{8}$$

$$\mathbf{B}(\mathbf{x}) = [w_1(\mathbf{x})\mathbf{p}(\mathbf{x}_1), w_2(\mathbf{x})\mathbf{p}(\mathbf{x}_2), \ldots, w_n(\mathbf{x})\mathbf{p}(\mathbf{x}_n)] \tag{9}$$

$$\mathbf{u} = [u_1, u_2, \ldots, u_n]^{\mathrm{T}} \tag{10}$$

Solving $\mathbf{a}(\mathbf{x})$ from Eq. (7), and substituting it into Eq. (5), the final form of the MLS approximation is expressed as

$$u^h(\mathbf{x}) = \sum_{I=1}^{n} N_I(\mathbf{x})\, u_I \tag{11}$$

where the shape function $N_I(\mathbf{x})$ is given by

$$N_I(\mathbf{x}) = \mathbf{p}^{\mathrm{T}}(\mathbf{x}) \cdot \mathbf{A}^{-1}(\mathbf{x}) \cdot \mathbf{B}_I(\mathbf{x}) \tag{12}$$

where $\mathbf{B}_I(\mathbf{x})$ denotes the Ith column of the matrix $\mathbf{B}(\mathbf{x})$.

Different from the finite-element approximation, the continuity of the MLS approximation relates to not only the basis function, but also the weight function. If the continuities of the basis functions and the weight function are C^l and C^k, respectively, then the continuity of the MLS shape function is $C^{\min(l,k)}$, which means that the weight function plays an important role in the MLS shape function since frequently used monomial bases are infinitely differentiable. Many kinds of weight functions [11] have been employed in meshless methods. In this article, the cubic spline function is adopted, which has the following form in the 1-D case:

$$w_I(r) = \begin{cases} \frac{2}{3} - 4r^2 + 4r^3 & r \le \frac{1}{2} \\ \frac{4}{3} - 4r + 4r^2 - \frac{4}{3}r^3 & \frac{1}{2} < r \le 1 \\ 0 & r > 1 \end{cases} \tag{13}$$

where $r = |x - x_I|/d^{\max}$, $d^{\max}$ is the radius of the compact support. For the 2-D case, a rectangular support is used, and the weight function is defined as the product of the weight functions in x and y direction, viz.,

$$w_I(\mathbf{x}) = w_I(r_x) \cdot w_I(r_y) \tag{14}$$

where $w_I(r_x)$ and $w_I(r_y)$ are both defined by Eq. (13), and $r_x = |x - x_I|/d_x^{\max}$, $r_y = |y - y_I| / d_y^{\max}$. The choice of $d^{\max}$ will be discussed in Section 4 by numerical examples.

3.2. MWLS Method for Steady-State Equations

Substituting the MLS approximation (11) into the governing equation (4) and boundary conditions (2) of the steady-state heat conduction problem results in residuals

$$\begin{aligned}
&\text{In } \Omega: && R_0 = \sum_{I=1}^{n} [k\nabla^2 N_I(\mathbf{x})] u_I + \rho Q \\
&\text{On } \Gamma_1: && R_1 = \sum_{I=1}^{n} N_I(\mathbf{x}) u_I - \bar{u} \\
&\text{On } \Gamma_2: && R_2 = \sum_{I=1}^{n} [k\mathbf{n} \cdot \nabla N_I(\mathbf{x})] u_I - \bar{q} \\
&\text{On } \Gamma_3: && R_3 = \sum_{I=1}^{n} [k\mathbf{n} \cdot \nabla N_I(\mathbf{x}) + h N_I(\mathbf{x})] u_I - h u_f
\end{aligned} \tag{15}$$

In the MWLS method, the above residuals are minimized in a least-squares manner, that is, the functional

$$\Pi = \int_{\Omega} R_0^2(\mathbf{x})\, d\Omega + \int_{\Gamma_1} \alpha_1 R_1^2(\mathbf{x})\, d\Gamma + \int_{\Gamma_2} \alpha_2 R_2^2(\mathbf{x})\, d\Gamma + \int_{\Gamma_3} \alpha_3 R_3^2(\mathbf{x})\, d\Gamma \tag{16}$$

is minimized, which is equivalent to

$$\frac{\partial \Pi}{\partial u_I} = 0 \qquad I = 1, 2, \ldots, N_{\text{node}} \tag{17}$$

where N_{node} is the total number of nodes, and α_l $(l = 1, 2, 3)$ are penalty parameters.

Note that an integral form is involved in Eq. (16), which will decrease the computational efficiency of the method due to the heavy work of numerical quadrature. Since the integration in Eq. (16) is used only to average the residuals, and the accuracy of the least-squares approach is much less sensitive to the integration accuracy than that of the Galerkin approach [16], an alternative discrete functional Π is used to avoid integration:

$$\Pi = \sum_{K=1}^{m_0} R_0^2(\mathbf{x}_K) + \sum_{K=1}^{m_1} \alpha_1 R_1^2(\mathbf{x}_K) + \sum_{K=1}^{m_2} \alpha_2 R_2^2(\mathbf{x}_K) + \sum_{K=1}^{m_3} \alpha_3 R_3^2(\mathbf{x}_K) \tag{18}$$

where m_0 and m_i $(i = 1, 2, 3)$ are the number of evaluation points to satisfy the governing equation and to enforce boundary conditions, respectively. It should be noticed that the number of evaluation points need not equal the number of nodes; in other words, the number of evaluation points can be larger than the number of nodes. According to research by Onate [25], considering the influence of the governing equations on the boundary will contribute to the stabilization of the algorithm. So, in the MWLS method, all the nodes are taken as evaluation points for the first term of summation; and the nodes on Γ_i are selected to be the evaluation points on corresponding boundaries.

Substituting the discrete functional Π of Eq. (18) into Eq. (17), the system equations of the MWLS method for solving steady-state heat conduction equations are obtained as

$$\mathbf{KU} = \mathbf{P} \tag{19}$$

where the matrices are defined as

$$\mathbf{U} = (u_1, u_2, \ldots, u_{N_{\text{node}}})^{\mathrm{T}} \tag{20}$$

$$K_{IJ} = \sum_{K=1}^{m_0} \left(k\nabla^2 N_I\right)\left(k\nabla^2 N_J\right)\big|_{\mathbf{x}_K} + \sum_{K=1}^{m_1} \alpha_1 N_I N_J\big|_{\mathbf{x}_K} + \sum_{K=1}^{m_2} \alpha_2 (\mathbf{n} \cdot k\nabla N_I) \times (\mathbf{n} \cdot k\nabla N_J)\big|_{\mathbf{x}_K} + \sum_{K=1}^{m_3} \alpha_3 (\mathbf{n} \cdot k\nabla N_I + hN_I)(\mathbf{n} \cdot k\nabla N_J + hN_J)\big|_{\mathbf{x}_K} \tag{21}$$

$$P_I = -\sum_{K=1}^{m_0}(k\nabla^2 N_I)\rho Q|_{\mathbf{x}_K} + \sum_{K=1}^{m_1}\alpha_1 N_I \bar{u}|_{\mathbf{x}_K} + \sum_{K=1}^{m_2}\alpha_2(\mathbf{n}\cdot k\nabla N_I)\,\bar{q}|_{\mathbf{x}_K} + \sum_{K=1}^{m_3}\alpha_3(\mathbf{n}\cdot k\nabla N_I + hN_I)\,hu_f|_{\mathbf{x}_K} \tag{22}$$

where the symbol $|_{\mathbf{x}_K}$ represents the value at $\mathbf{x} = \mathbf{x}_K$.

In fact, the above routine process of implementation of the MWLS method can be extended to any boundary-value problems as described below.

1. Substitute a meshless approximation, such as the MLS approximation, Eq. (11), into the governing equations and boundary conditions. Residuals in the domain and on the boundaries are obtained.
2. Construct the functional Π by summation of the squares of the residuals. In order to avoid integration, the functional in discrete form can be used.
3. Minimize the functional Π, which is equivalent to that the variation of Π equals zero, to obtain the discretized equations.
4. Solve the discretized equations to obtain nodal parameters u_I, then calculate other variables required.

In the above discretizing process, the boundary conditions are introduced in a penalty manner. In fact, the penalty parameters α_l $(l = 1, 2, 3)$ have two functions. One is to make the residuals of the boundary conditions much larger than that of the governing equation, so that the boundary conditions can be satisfied accurately; the other is to balance the orders of magnitude of different boundary residuals. For the first purpose, the penalty parameters should be large numbers. For the second purpose, a direct and simple dimensional analysis has been applied to the residuals of different boundary conditions to find if the following relations $\alpha_1 = \alpha_2(k/L)^2$ and $\alpha_3 = \alpha_2\,[\min(1, k/hL)]^2$ are satisfied, different boundary residuals will be of the same or close order of magnitude. Note that the parameter α_2 is taken as a reference value. We have examined different values of α_2 and found that the results are nearly the same when the order of magnitude of α_2 is not less than 10^5. Since extremely large penalty parameters will lead to an ill-conditioned system matrix, a value of 10^5–10^8 for α_2 is recommended in the MWLS method.

3.3. Extending to Unsteady-State Problems

The unsteady-state heat conduction problem, Eq. (1), involves the time derivative. Thus some algorithm to discretize the time domain should be employed. In the Galerkin FEM or GBMM, a common approach is first to discretize the space domain to obtain ordinary differential equations (ODEs) with respect to time; then to solve the ODEs to trace the variance of temperature with time step by step. This process does not suit the MWLS method, since the squares of the time derivative will be involved. Another approach, adopted in least-squares FEM [26], is used in this article as follows.

First discretize Eq. (1) in the time domain by the θ method, which leads to

$$\rho c \frac{u^{n+1} - u^n}{\Delta t} = \theta\left(k\nabla^2 u + \rho Q\right)^{n+1} + (1-\theta)\left(k\nabla^2 u + \rho Q\right)^n \tag{23}$$

where the parameter $0 \le \theta \le 1$, and $0, \frac{1}{2}, 1$ correspond to the forward difference, the central difference, and the backward difference algorithms. The superscript n indicates the value at the nth time step. The above equation can be rewritten as

$$\left(\frac{\rho c}{\Delta t} - \theta k\nabla^2\right)u^{n+1} = \left[\frac{\rho c}{\Delta t} + (1-\theta)k\nabla^2\right]u^n + \rho Q^{n+\theta} \tag{24}$$

where $Q^{n+\theta} = \theta Q^{n+1} + (1-\theta)Q^n$. The terms on the right-hand side of Eq. (24) at the $(n+1)$th time step can be determined completely by the results of the nth step and the prescribed conditions. Thus Eq. (24) and the boundary conditions (2) constitute boundary-value problems for the unknown nodal parameters at the $(n+1)$th step, which can be solved by the MWLS method. Following the routine process of the MWLS method to solve boundary-value problems, as described at the end of Section 3.2, the discretized equations for unsteady-state heat conduction problems are derived as

$$\mathbf{K}\mathbf{U}^{n+1} = \mathbf{G}\mathbf{U}^n + \mathbf{P} \tag{25}$$

where

$$\begin{aligned} K_{IJ} = & \sum_{K=1}^{m_0}\left(\frac{\rho c}{\Delta t}N_I - \theta k\nabla^2 N_I\right)\left(\frac{\rho c}{\Delta t}N_J - \theta k\nabla^2 N_J\right)\Big|_{\mathbf{x}_K} \\ & + \sum_{K=1}^{m_1}\alpha_1 N_I N_J|_{\mathbf{x}_K} + \sum_{K=1}^{m_2}\alpha_2(\mathbf{n}\cdot k\nabla N_I)(\mathbf{n}\cdot k\nabla N_J)|_{\mathbf{x}_K} \\ & + \sum_{K=1}^{m_3}\alpha_3(\mathbf{n}\cdot k\nabla N_I + hN_I)(\mathbf{n}\cdot k\nabla N_J + hN_J)|_{\mathbf{x}_K} \end{aligned} \tag{26}$$

$$G_{IJ} = \sum_{K=1}^{m_0}\left(\frac{\rho c}{\Delta t}N_I - \theta k\nabla^2 N_I\right)\left[\frac{\rho c}{\Delta t}N_J + (1-\theta)k\nabla^2 N_J\right]\Big|_{\mathbf{x}_K} \tag{27}$$

$$\begin{aligned} P_I = & \sum_{K=1}^{m_0}\left(\frac{\rho c}{\Delta t}N_I - \theta k\nabla^2 N_I\right)\rho Q^{n+\theta}\Big|_{\mathbf{x}_K} + \sum_{K=1}^{m_1}\alpha_1 N_I \bar{u}^{n+1}|_{\mathbf{x}_K} \\ & + \sum_{K=1}^{m_2}\alpha_2(\mathbf{n}\cdot k\nabla N_I)\bar{q}^{n+1}|_{\mathbf{x}_K} + \sum_{K=1}^{m_3}\alpha_3(\mathbf{n}\cdot k\nabla N_I + hN_I)hu_f^{n+1}|_{\mathbf{x}_K} \end{aligned} \tag{28}$$

It is well known that the forward difference algorithm is conditionally stable, and the critical size of time step is related to the node distribution. Smolinski and

Palmer [27] have studied the critical size of time step for the FEM and EFGM in 1-D diffusion problems. They give a rough estimate as

$$\Delta t_c^{\mathrm{EFGM}} = \frac{L_e d^{\max}}{2} \qquad \Delta t_c^{\mathrm{FEM}} = \frac{L_e^2}{2} \tag{29}$$

where L_e is the element dimension in the FEM and the nodal distance in the EFGM, respectively. In fact, this conclusion is also correct for other GBMMs, and it can be extended to the analysis of other meshless methods similarly. As the essence of constructing discrete functional Π in the MWLS method is analogous to nodal integration, a rough estimate of critical time step size for the MWLS method can be obtained according to Smolinski and Palmer's work:

$$\Delta t_c^{\mathrm{MWLS}} = \frac{(d^{\max})^2}{2} \tag{30}$$

which implies that the ratio of critical step size of the MWLS method to that of the EFGM is about $d^{\max}/L_e$, whose typical value is $1.0 < d^{\max}/L_e \leq 4.0$ in meshless methods. The penalty parameters can be selected in the same way as in the steady-state case.

4. NUMERICAL EXAMPLES

In all the following examples, thermophysical parameters, such as density, specific heat, and thermal conductivity, are unit values if not explicitly specified.

4.1. 1-D Steady-State Example and Choice of Parameters

Consider an infinitely large slab as shown in Figure 1. The left surface of the slab is maintained at the temperature 100°C. Forced-convection heat transfer occurs at the other surface with the fluid temperature 0°C. There exists a distributed heat source $Q = 180x^2$ along the thickness of the slab, where x is the distance to the left surface, as shown in Figure 1. The thickness of the slab is 1 m. This example is a 1-D problem in essence, and its analytical solution is

$$u = -15x^4 - 12.5x + 100 \tag{31}$$

This example is studied for optimal choice of computational parameters and convergence analysis. Table 1 lists the relative error of different orders of monomial bases and different support radii, where *scale* refers to the ratio of support radius to nodal distance. The relative error is defined as

$$E_r = \frac{\sqrt{\sum_{I=1}^{N_{\mathrm{node}}} (u_I^{\mathrm{num}} - u_I^{\mathrm{e}})^2}}{\sqrt{\sum_{I=1}^{N_{\mathrm{node}}} (u_I^{\mathrm{e}})^2}} \tag{32}$$

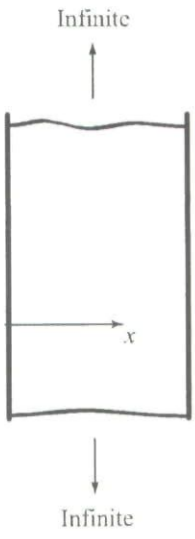

Figure 1. An infinitely large slab.

where the superscripts num and e denote numerical results of the MWLS method and exact solution Eq. (31), respectively. As seen from the table, quadratic basis gives the best results, which is not surprising since the highest order of derivative in the functional Π is 2. Linear basis and constant basis can also give satisfactory results with certain support radius, mainly because the performances of MLS shape functions is related to both the basis functions and the weight function, and the spline function with high smoothness as C^2 continuity is adopted as weight function in this article. In the following examples, the quadratic basis with a support size of 3.5 times the nodal distance is used.

Figure 2 shows the convergence curve of the MWLS method and the GBMM, where GBMMn means results of the GBMM with n-point Gauss quadrature. The accuracy of the MWLS method is higher than that of GBMM1 and close to that of GBMM2, but the convergence rate of the MWLS method is much higher than that of the GBMM, no matter how many integration points are used. Note that more integration points imply more computational cost, which is especially remarkable in 2-D or 3-D problems.

Table 1. Relative error of MWLS results with different computational parameters (%)

Scale	Constant basis	Linear basis	Quadratic basis
2.25	21.87	2.044	0.4740
2.5	15.15	0.2694	0.5978
2.75	11.12	0.9572	0.6123
3.0	7.667	1.649	0.5740
3.25	3.971	0.5003	0.2070
3.5	2.216	1.262	0.0692
3.75	1.218	1.253	0.2071
4.0	0.7748	0.7892	0.3398

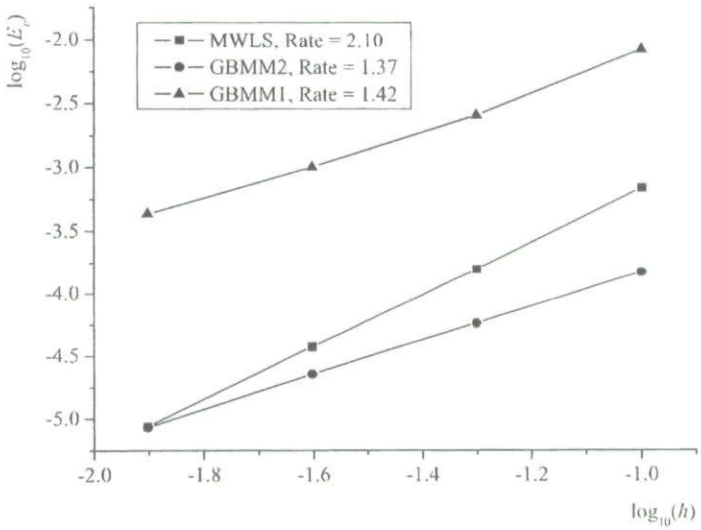

Figure 2. Convergence curve of 1-D steady-state example.

Another case in which a uniform heat flux is applied at the right surface is also investigated, and the same conclusion can be drawn.

4.2. Steady-State Heat Conduction in a Rectangular Domain

A rectangular domain in the dimension $1\,\mathrm{m} \times 0.8\,\mathrm{m}$ is shown in Figure 3. The upper boundary is subject to an inflow heat flux of magnitude $\bar{q} = 500\,\mathrm{W/m^2}$, all the other boundaries are maintained at the temperature 0°C, and no source exists in the domain. The thermal conductivity is $1.2\,\mathrm{W/(m°C)}$. The analytical solution is [28]

$$u(x,y) = \frac{4\bar{q}a}{k\pi^2} \sum_{m=0}^{\infty} \frac{\sinh\left\{\left[\frac{(2m+1)\pi}{a}\right] y\right\}}{\cosh\left\{\left[\frac{(2m+1)\pi}{a}\right] b\right\}} \frac{\sin\left\{\left[\frac{(2m+1)\pi}{a}\right] x\right\}}{(2m+1)^2} \tag{33}$$

The isothermals of the GBMM and MWLS method are shown in Figures 4 and 5, respectively. In the computation, a support size of 2.5 times the nodal distance, the linear monomial basis, and 3×3 Gauss quadrature are employed in the GBMM; 11×9 uniform node distribution is used in both methods. The relative error of the MWLS is lower than that of the GBMM, is 1.21% versus 1.75%. Convergence analysis shows that the rate of the MWLS method is a little lower than that of the GBMM, as plotted in Figure 6. However, the CPU time for the MWLS is less than 20% of that of the GBMM, 18.4% for 11×9 and 16.0% for 21×17 uniform node distributions, respectively.

From this example and the previous one, it can be seen that the MWLS method is a promising meshless method when both the accuracy and efficiency are taken into account.

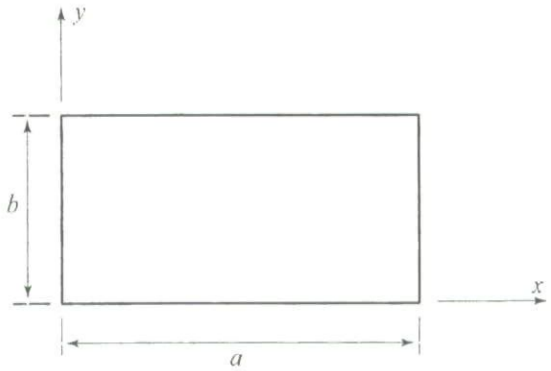

Figure 3. Rectangular domain and its coordinate system.

4.3. 1-D Unsteady-State Examples

Consider the unsteady-state heat conduction in an infinite slab whose thickness is 2 m. The temperatures of both surfaces are 0°C, and the initial temperature distribution has the form $u_0 = x(2 - x)$. The analytical solution is given by [28]

$$u(x,t) = \frac{16}{\pi^3}\sum_{n=1}^{\infty}\frac{1-(-1)^n}{n^3}\exp\left(-\frac{n^2\pi^2}{4}t\right)\sin\left(\frac{n\pi}{2}x\right) \tag{34}$$

Only one-half of the domain needs to be analyzed due to symmetry, and the adiabatic boundary condition is enforced on the symmetrical line. Figure 7 shows the results of the GBMM, the MWLS method, and the analytical solution on the sym-

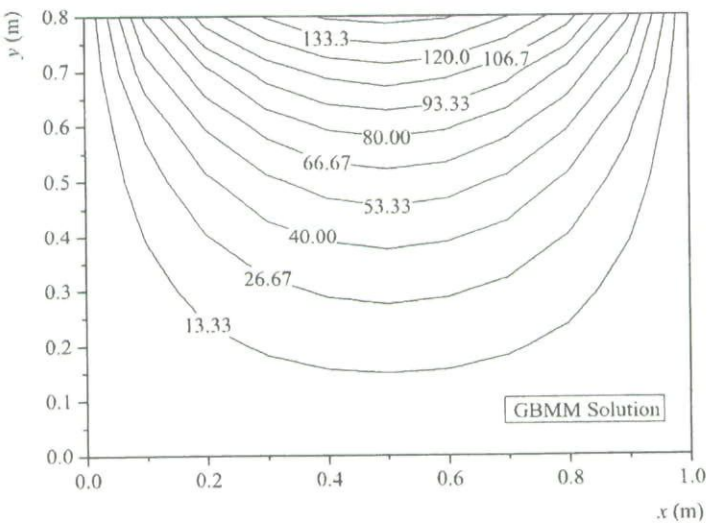

Figure 4. Isothermal of 2-D steady-state example (°C): GBMM results.

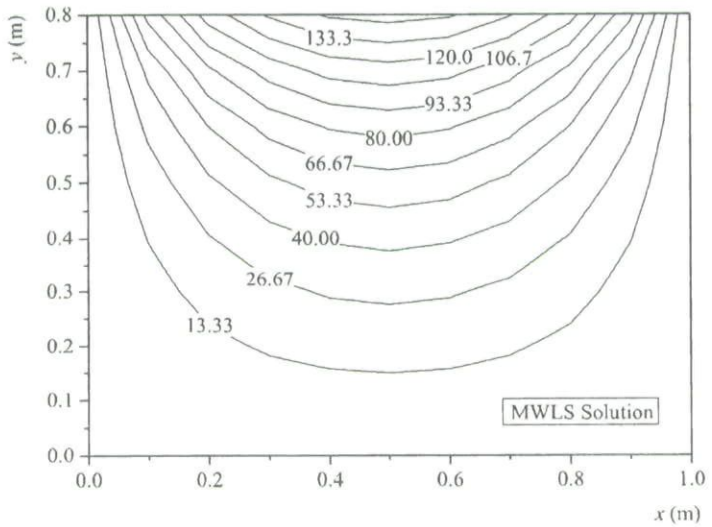

Figure 5. Isothermal of 2-D steady-state example (°C): results of MWLS method.

metrical line. Eleven uniformly distributed nodes are employed in the computation, the size of the time step is 0.05 s, and the cases $\theta = \frac{1}{2}$ and 1 are both computed. All the numerical results coincide well, and in fact cannot be distinguished from the analytical solution when $\theta = \frac{1}{2}$. The result of the central difference algorithm is more accurate than that of the backward difference algorithm, owing to second-order accuracy.

Figure 8 shows the temperature variance on the symmetrical line computed by the MWLS method when $\theta = 0$ and the size of the time step $\Delta t = 0.002$ s. The result

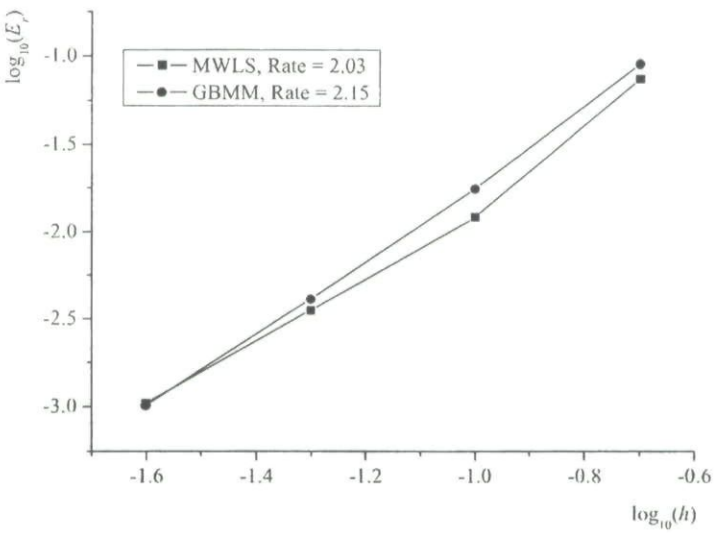

Figure 6. Convergence curve of 2-D steady-state example.

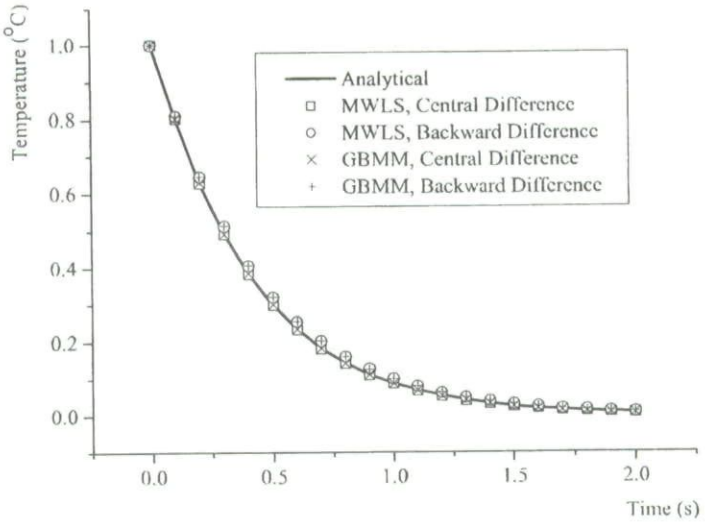

Figure 7. Comparison of analytical solution and numerical results on the symmetrical line when $\theta = 0.5$ and 1.0.

of the GBMM diverges for this time-step size, so it is not drawn in the figure. Further computation shows that the critical step size of the MWLS method is 2.5×10^{-3} s, while that of the GBMM is 7.0×10^{-4} s. The ratio of critical time-step size of the MWLS method to that of the GBMM is about 3.6, which is consistent with the theoretical analysis in Section 3.3.

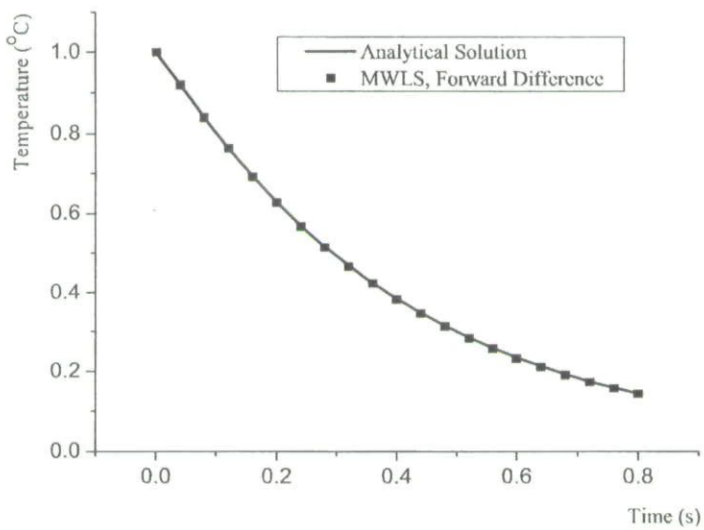

Figure 8. Comparison of analytical solution and numerical results on the symmetrical line when $\theta = 0$.

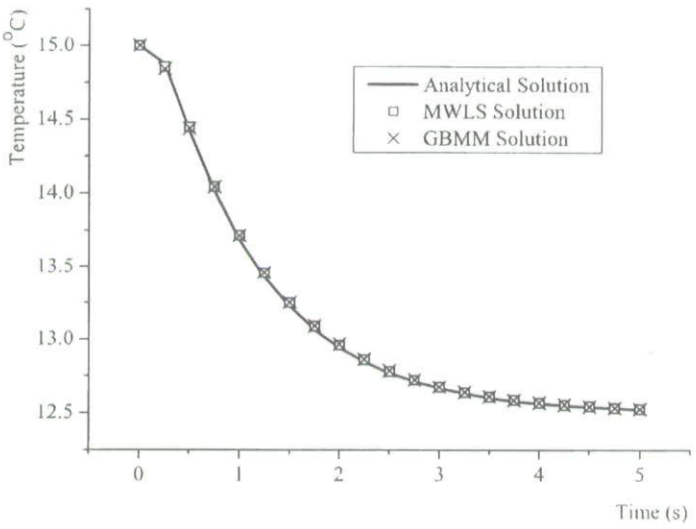

Figure 9. Variance of temperature on the central line.

Consider another example in which the temperatures of the left and the right surface are $U_1 = 15°C$ and 10°C, respectively. The thickness is 1 m, and the thermal conductivity is 0.1 W/m°C. The initial temperature is $U_0 = 15°C$ throughout the domain. The variance of temperature with space coordinate and time is described

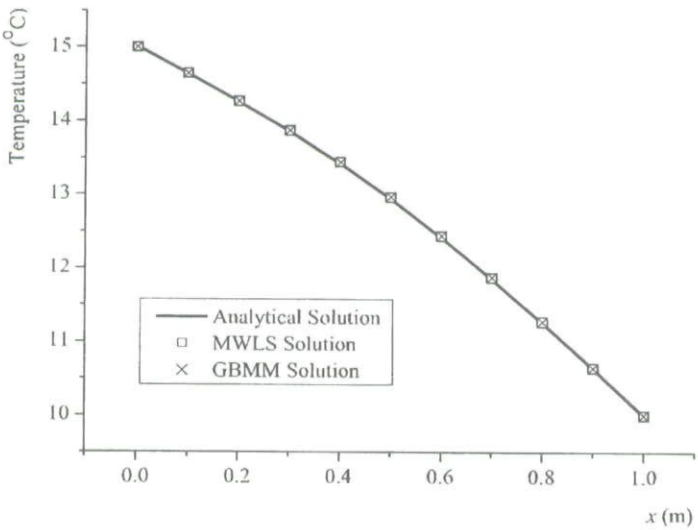

Figure 10. Temperature distribution along the thickness direction at $t = 2$ s.

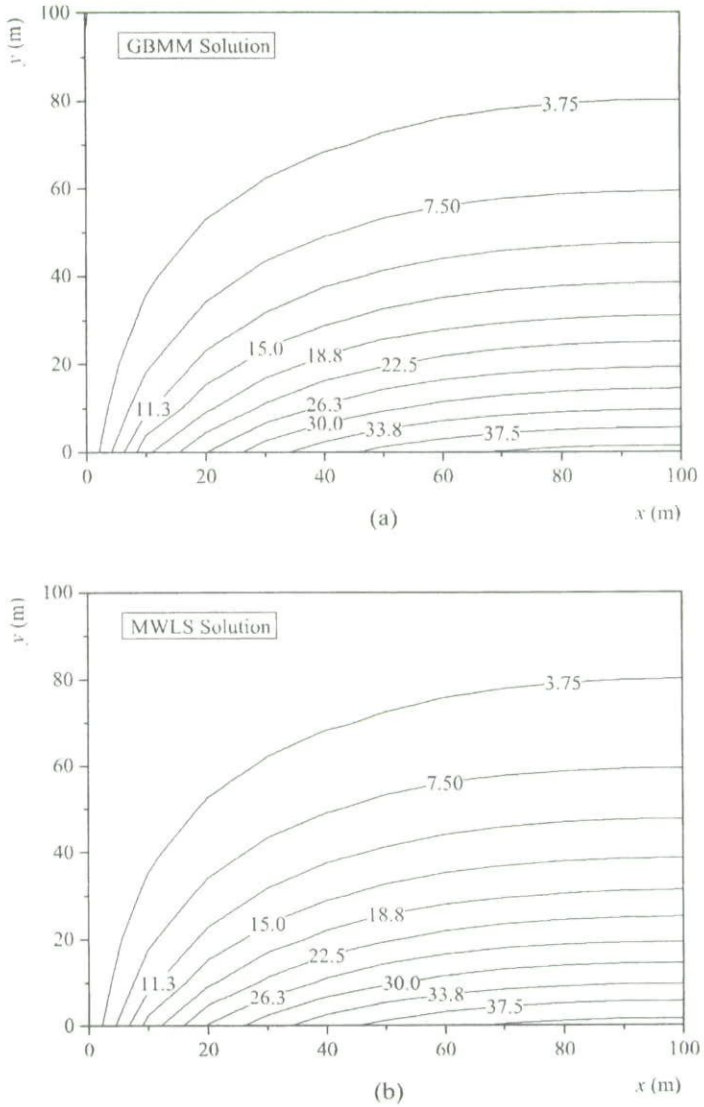

Figure 11. Comparison of the isothermal (°C) at $t = 1.5$ s: (*a*) results of GBMM; (*b*) results of MWLS method.

in the series form [28]

$$u(x,t) = U_1 + (U_2 - U_1)\frac{x}{l} + \frac{2}{\pi}\sum_{n=1}^{\infty}\frac{1}{n}\left[(U_0 - U_1)\left[1 - (-1)^n\right] + (-1)^{n+1}(U_1 - U_2)\right] \times \exp\left(-\frac{n^2\pi^2 a^2}{l^2}t\right)\sin\left(\frac{n\pi x}{l}\right) \tag{35}$$

where $a^2 = k/\rho c$. Eleven uniformly distributed nodes are used in the computation,

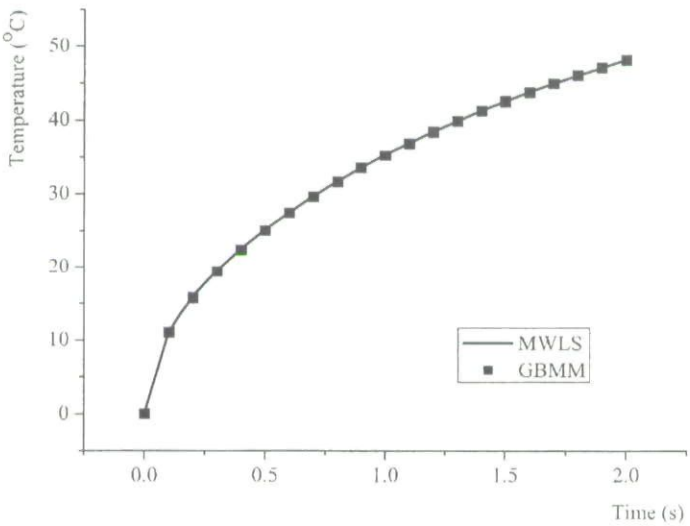

Figure 12. Variance of temperature on point A.

the time-step size $\Delta t = 0.05\,\text{s}$, and $\theta = \frac{1}{2}$. The variance of temperature on the central line is shown in Figure 9, and the temperature along the x axis at $t = 2\,\text{s}$ is given in Figure 10. As can be seen, the results of the MWLS method agree well with the analytical solution and the results of the GBMM.

4.4. 2-D Unsteady-State Example

The length and width of the rectangular domain in Figure 3 both equal 100 m. The left boundary is maintained at temperature 0°C, a heat flux of magnitude $1{,}000\,\text{W/m}^2$ enters the domain from the bottom, and the other boundaries are insulated. The thermal conductivity is $1{,}000\,\text{W/m°C}$. The initial temperatures in the entire domain are 0°C. 11×11 nodes are used in the computation with the parameter $\theta = 1.0$ and the time-step size $\Delta t = 0.01\,\text{s}$. Figure 11 plots the isothermal of the MWLS method and the GBMM at time $t = 1.5\,\text{s}$, and Figures 12 and 13 give the variance of temperatures at points A ($x = 100$, $y = 0$) and B ($x = 100$, $y = 50$).

5. CONCLUSION

In this article, a novel meshless method based on the least-squares approach, the meshless weighted least-squares (MWLS) method, is extended to solve conduction heat transfer problems. A discrete functional is employed in the MWLS method to construct a set of linear equations, which avoids the burdensome task of numerical integration. Different time-stepping algorithms are combined with the MWLS method to solve unsteady-state heat conduction problems.

1-D and 2-D examples show that the accuracy and the convergence rate of the MWLS method are close to, or even better than, those of the GBMM. However, the MWLS method is much less time-consuming than the GBMM. Moreover, when

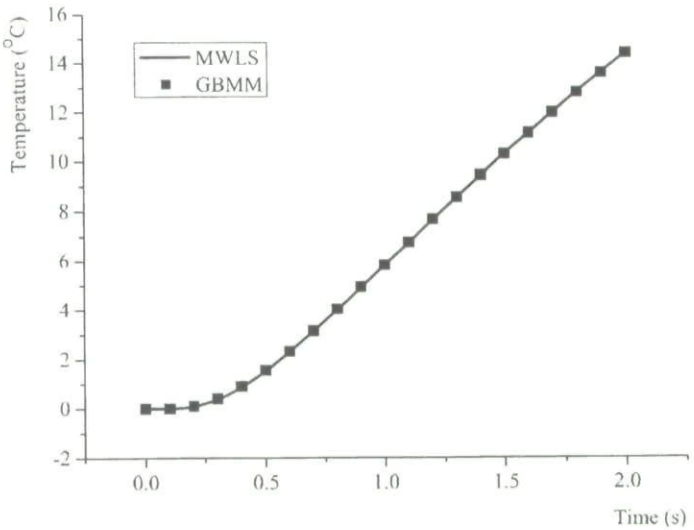

Figure 13. Variance of temperature on point *B*.

solving unsteady-state problems with an explicit algorithm, a larger time step can be adopted in the MWLS method. When the computational accuracy and efficiency are both taken into consideration, the MWLS method may be a promising meshless method.

Further research will be applications of the MWLS method in more practically complicated problems and in convection heat transfer problems.

REFERENCES

1. T. Belytschko, Y. Krongauz, D. Organ, M. Fleming, and P. Krysl, Meshless Methods: An Overview and Recent Developments, *Comput. Meth. Appl. Mech. Eng.*, vol. 139, pp. 3–47, 1996.
2. S. Li and W. K. Liu, Meshfree and Particle Methods and Their Applications, *Appl. Mech. Rev.*, vol. 55, pp. 1–34, 2002.
3. P. W. Cleary and J. J. Monaghan, Conduction Modelling Using Smoothed Particle Hydrodynamics, *J. Comput. Phys.*, vol. 148, pp. 227–264, 1999.
4. J. K. Chen, J. E. Beraun, and T. C. Carney, A Corrective Smoothed Particle Method for Boundary Value Problems in Heat Conduction, *Int. J. Numer. Meth. Eng.*, vol. 46, pp. 231–252, 1999.
5. E. Onate, S. Idelsohn, O. C. Zienkiewicz, and R. L. Taylor, A Finite Point Method in Computational Mechanics: Application to Convective Transport and Fluid Flow, *Int. J. Numer. Meth. Eng.*, vol. 39, pp. 3839–3866, 1996.
6. W. Chen, High-Order Fundamental and General Solutions of Convection-Diffusion Equation and Their Applications with Boundary Particle Method, *Eng. Anal. Bound. Elem.*, vol. 26, pp. 571–575, 2002.
7. Y. Liu and H. T. Yang, A Combined Approach of EFG/FE-EFG Methods and Precise Algorithm in Time Domain Solving Heat Conduction Problems, *J. Basic Sci. Eng.*, vol. 10, pp. 307–317, 2002 (in Chinese).

8. I. V. Singh, K. Sandeep, and R. Prakash, Heat Transfer Analysis of Two-Dimensional Fins Using Meshless Element-Free Galerkin Method, *Numer. Heat Transfer A*, vol. 44, no. 1, pp. 73–84, 2003.
9. I. V. Singh, K. Sandeep, and R. Prakash, The Element Free Galerkin Method in Three-Dimensional Steady State Heat Conduction, *Int. J. Comput. Eng. Sci.*, vol. 3, no. 3, pp. 291–303, 2002.
10. I. V. Singh and R. Prakash, The Numerical Solution of Three-dimensional Transient Heat Conduction Problems Using Element Free Galerkin Method, *Int. J. Heat Tech.*, vol. 21, no. 2, pp. 73–80, 2003.
11. I. V. Singh, A Numerical Solution of Composite Heat Transfer Problems Using Meshless Method, *Int. J. Heat Mass Transfer*, vol. 47, no. 10–11, pp. 2123–2138, 2004.
12. H. Sadat and S. Couturier, Performance and Accuracy of a Meshless Method for Laminar Natural Convection, *Numer. Heat Transfer B*, vol. 37, pp. 355–467, 2000.
13. T. Sophy, H. Sadat, and C. Prax, A Meshless Formulation for Three-Dimensional Laminar Natural Convection, *Numer. Heat Transfer B*, vol. 41, pp. 433–445, 2002.
14. T. Belytschko, Y. Y. Lu, and L. Gu, Element Free Galerkin Method, *Int. J. Numer. Meth. Eng.*, vol. 37, pp. 229–256, 1994.
15. S. Beissel and T. Belytschko, Nodal Integration of the Element-Free Galerkin Method, *Comput. Meth. Appl. Mech. Eng.*, vol. 139, pp. 49–74, 1996.
16. S. H. Park and S. K. Youn, The Least-Square Meshfree Method, *Int. J. Numer. Meth. Eng.*, vol. 52, pp. 997–1012, 2001.
17. X. Zhang, X.-H. Liu, K.-Z. Song, and M.-W. Lu, Least-Square Collocation Meshless Method, *Int. J. Number. Meth. Eng.*, vol. 51, pp. 1089–1100, 2001.
18. J. T. Chen, M. H. Chang, and K. H. Chen, and I. L. Chen, Boundary Collocation Method for Acoustic Eigenanalysis of Three-Dimensional Cavities Using Radial Basis Function, *Comput. Mech.*, vol. 29, pp. 392–408, 2002.
19. W. Chen, Symmetric Boundary Knot Method, *Eng. Anal. Bound. Elem.*, vol. 26, pp. 489–494, 2002.
20. W. Chen and Y. C. Hon, Numerical Convergence of Boundary Knot Method in the Analysis of Helmholtz, Modified Helmholtz, and Convection-Diffusion Problems, *Comput. Meth. Appl. Mech. Eng.*, vol. 192, pp. 1859–1875, 2003.
21. X. Zhang, K.-Z. Song, and M.-W. Lu, Meshless Methods Based on Collocation with Radial Basis Functions, *Comput. Mech.*, vol. 26, pp. 333–343, 2000.
22. B. N. Jiang, *The Least-Squares Finite Element Method: Theory and Applications in Computational Fluid Dynamics and Electromagnetics*, chap. 1, Springer-Verlag, Berlin, 1998.
23. X. Zhang, X. F. Pan, W. Hu, and M. W. Lu, Meshless Weighted Least-Square Method, *Fifth World Congress on Computational Mechanics*, Vienna, Austria, 2002, http://wccm.tuwien.ac.at.
24. W. Hu, Least Square Meshless Method on Nonlinear Dynamical Problems of Wave and Impact, M.E. thesis, Tsinghua University, Beijing, China, 2003.
25. E. Onate, F. Perazzo, and J. Miquel, A Finite Point Method for Elasticity Problems, *Comput. Struct.*, vol. 79, pp. 2151–2163, 2001.
26. B. N. Jiang, *The Least-Squares Finite Element Method: Theory and Applications in Computational Fluid Dynamics and Electromagnetics*, pp. 170–171, Springer-Verlag, Berlin, 1998.
27. P. Smolinski and T. Palmer, Procedures for Multi-Time Step Integration of Element-Free Galerkin Methods for Diffusion Problems, *Comput. Struct.*, vol. 77, pp. 171–183, 2000.
28. B. M. Budak, A. A. Samarskii, and A. H. Tikhenev, *A Collection of Problems on Mathematical Physics*, translated by A. R. M. Robson, pp. 331, 332, 456, Pergamon Press, New York, 1964.